Pergamon

0043-1354(94)00186-3

Wat. Res. Vol. 29, No. 2, pp. 443–453, 1995

0043-1354/95 $7.00 + 0.00

FRACTAL DIMENSIONS OF AGGREGATES FORMED IN DIFFERENT FLUID MECHANICAL ENVIRONMENTS

BRUCE E. LOGAN*Ⓜ and JOHN R. KILPS

Environmental Engineering Program, Department of Chemical and Environmental Engineering, University of Arizona, Tucson, AZ 85721, U.S.A.

(First received November 1993; accepted in revised form July 1994)

Abstract—The fractal properties of aggregates formed under two different fluid mechanical environments, a paddle mixer and a rolling cylinder, were measured using three different techniques: a non-steady state method requiring both volume and length size distributions, a steady state size distribution method, and an aggregate property scaling method. Based on cumulative size distributions and the non-steady state method, aggregates produced in the rolling cylinder had a fractal dimension of $D_3(l,v) = 1.59 \pm 0.16$, while aggregates produced in the paddle mixer had a higher fractal dimension of $D_3(l,v) = 1.92 \pm 0.04$. Fractal dimensions calculated assuming steady state size distributions based on aggregate volume were substantially different than those based on aggregate length indicating that size distributions in both devices were not at steady state during the experiment. Although fractal dimension based on cumulative size distributions were similar in magnitude to those calculated using discrete and data-averaged size distributions, the cumulative size distributions produced fractal dimensions with the lowest errors. When $D_3 < 2$, three dimensional and two dimensional fractal dimensions should be equal. Power law equations for two dimensional fractal dimensions based on aggregate properties (length and area) were in good agreement with three dimensional fractal dimensions. Rolling cylinder and paddle mixer aggregates had two dimensional fractal dimensions of $D_2 = 1.68 \pm 0.02$ and $D_2 = 1.89 \pm 0.02$. These experiments demonstrate that aggregate properties are a function of the fluid mechanical environment used to coagulate particles.

Key words—coagulation, marine snow, particles, shear, size distributions

INTRODUCTION

The coagulation of oceanic particles into large, fast settling aggregates can dominate the mass of sedimenting material in marine systems (Fowler and Knauer, 1986; Alldredge and Silver, 1988; Jackson, 1990) making coagulation processes critical to modeling oceanic carbon fluxes. These large (>0.5 mm) aggregates, called marine snow, are either classified as a specific type of aggregate, according to the predominant particle type of particle (diatoms, fecal pellets, or larvacean houses) or as "miscellaneous" aggregates composed of unidentifiable material from the water column (Alldredge and Gotschalk, 1988; Kilps *et al.*, 1993). Although the composition of marine snow aggregates has been extensively studied, the physical mechanisms generating marine snow aggregates are not well understood. Particle collisions necessary to produce aggregates can be generated by Brownian motion, fluid shear, and differential sedimentation (McCave, 1975; Hunt, 1980). Brownian motion is generally acknowledged to be important only for small particles (< 1 μm) in the ocean. Both shear and differential sedimentation have been suggested to predominate in the coagulation of particles into larger aggregates (McCave, 1975; Hunt, 1980; Jackson, 1990; Hill, 1992), but no direct method for determining the critical collision mechanism for large aggregate formation in the ocean has been found.

Fractal geometry has been used to describe the morphology of highly irregular objects by characterizing the object imbedded onto two- and three-dimensional space using fractal dimensions defined here as two- and three-dimensional fractal dimensions. For aggregates formed by Brownian motion the magnitude of two- and three-dimensional fractal dimensions, D_2 and D_3, is independent of the type of colloidal particle (clay, polymer or gold), but dependent on particle stickiness. Highly destabilized (very sticky) particles have fractal dimensions of 1.8, while less destabilized particles have higher fractal dimensions of 2.2 (Lin *et al.*, 1989). There is no evidence of a similar universality of these fractal dimensions for aggregates formed by other mechanisms (Logan and Wilkinson, 1990). Aggregates in marine systems formed from diatoms, fecal pellets, and unidentifiable miscellaneous debris in the water column have lower fractal dimensions in the range of $1.28 \leq D_2 \leq 1.86$ (Kilps *et al.*, 1994), and inorganic aggregates produced by paddle mixers may have fractal dimensions of $1.4 \leq D_3 \leq 2.85$ (Li and Ganczarczyk, 1989).

*Author to whom all correspondence should be addressed.

The variability of the fractal dimensions for marine snow aggregates could result from differences in particle stickiness, coagulation mechanisms forming the aggregates (shear or differential sedimentation), and composition of the particles composing the aggregate. An understanding of the extent that these different factors affect aggregate morphology, and therefore the fractal dimensions, has not emerged because of a variety of methods used to analyze the aggregates, the different types of particles forming the aggregates, and a lack of consistent coagulation conditions. A variety of experimental conditions have been used in an attempt to simulate fluid mechanical conditions in the ocean, including paddle mixers, oscillating grids, rotating cylinders (concentric cylinders, or couette devices) and rolling cylinders (Pasciak and Gavis, 1975; Shanks and Edmondson, 1989; Kiørboe *et al.*, 1990; Alldredge *et al.*, 1993). Each of these methods suffers from limitations and no one system has emerged as an experimental preference to produce aggregates representative of natural conditions.

Paddle mixers generate turbulent shear, are easy to operate and sample, and are routinely used by engineers to study coagulation processes and to generate aggregates. Fractal dimensions of aggregate formed in paddle mixers can be estimated from aggregate properties (size vs. settling velocity or porosity; e.g. Li and Ganczarczyk 1989 and references therein), but these fractal dimensions appear to be a function of experimental parameters such as particle type and solution chemistry. Rolling cylinders were first used by Shanks and Edmondson (1989) to coagulate seawater into aggregates with the same characteristics (size, composition and porosity) as naturally formed marine snow aggregates from the same location. This device consists of a cylindrical container completely filled with water that is set to rotate horizontally at a few revolutions per minute about its center at a slow rate. After some initial period of time the fluid rotates as a solid body (Tooby *et al.*, 1977; Jackson, 1994) and there should be no coagulation by fluid shear. Particles moving with the fluid can only collide with each other due to differential sedimentation. However, Jackson (1994) has pointed out that the initial period of rotation can induce substantial fluid shear and that particles will experience collisions with the container wall. While the mechanism of aggregate formation in rollers is complicated, the rolling cylinder device is still used by many researchers due to the rapid formation of marine snow like aggregates. The fractal dimensions of aggregates formed in rolling cylinders, however, has not been previously investigated or compared to aggregates formed in natural systems.

In order to show that the fluid mechanical environment affects aggregate morphology, and therefore the fractal dimensions, of aggregates produced by coagulation, we measured several properties of aggregates formed from a single source of particles in two different coagulation devices: a paddle mixer and a rolling cylinder. Three different techniques were used to calculate fractal dimensions: aggregate property scaling, steady state size distributions, and a dual-instrument multiple-size distribution technique. By limiting aggregate composition to only one type of particle, and by using the same techniques to analyze aggregates formed in the two different reactors, we were able to determine the extent that different fluid mechanical environments influenced the fractal dimensions and morphologies of the aggregates. Since we used a size distribution to calculate fractal dimensions, these results represent a statistical average for the whole population of aggregates formed in these devices and not just the properties of a few aggregates isolated from the population of coagulated particles.

METHODS

Theoretical

The geometrical properties and methods used to analyze fractal aggregates have been presented in detail elsewhere (Logan and Wilkinson, 1990, 1991; Jiang and Logan, 1991; Jiang, 1994; Kilps *et al.*, 1994) but are reviewed briefly here.

Fractal dimensions relate aggregate size to some property in n-dimensions, where $n = 1$, 2 or 3, and D_n is the fractal dimension in n-dimensions. For example, fractal dimensions of aggregates imbedded in two- and three-dimensions are:

$$A \propto l^{D_2} \tag{1}$$

$$N_p \propto l^{D_3}, \tag{2}$$

where l is the maximum aggregate size, A the projected aggregate area, and N_p the number of particles in the aggregate. The subscript n also indicates the value of the aggregate characteristic if it obeyed Euclidean geometry. A fractal dimension describing the perimeter of an object is frequently measured using a box method (Burrough, 1989; Kaye, 1989) by varying the size of a grid box, λ, and determining the number of grid boxes that cover the aggregate boundary, N_b. By this method, a one-dimensional fractal dimension, D_{1b}, is:

$$N_b \propto \lambda^{-D_{1b}}. \tag{3}$$

The perimeter of a population of particles can be analyzed using automated techniques that provide the perimeter of objects based on a single length scale (a single pixel for a computerized image). Thus, instead of changing the length scale of the measuring device, the sizes of the objects change. A one-dimensional fractal dimension can, therefore, be calculated for all particles in the distribution as:

$$P \propto l^{D_1}, \tag{4}$$

where P is the aggregate perimeter.

Since these different fractal dimensions characterize how the aggregate properties change with size, their magnitude is related to aggregate morphology. For example, aggregates with highly irregular perimeters have D_1 values greater than unity. Similarly, aggregates tend to become more porous with increasing size resulting in two- and three-dimensional fractal dimensions that are usually less than their corresponding integer values. Properties of aggregates that affect sedimentation rates, such as porosity, density, and sinking velocity, are primarily a function of D_2 and D_3. These fractal dimensions can also be calculated using the scaling relationships in Table 1. Since a whole population of aggregate are used in these calculations, the calculated fractal dimensions represent a statistical average for the population of aggregates. Individual aggregates may have higher or lower fractal dimensions.

When the three-dimensional fractal dimension is less than 2, then $D_3 = D_2$ (Meakin, 1988). This property of fractal aggregates allows direct comparison of different methods if $D_3 \leq 2$. Based on equation (3) and (4), the following proportionality can be calculated:

$$A \propto N_p^{D_2/D_3}. \tag{5}$$

Equation (5) was used to test whether the slope D_2/D_3 was equal to unity when $D_3 < 2$ by comparing the number of primary particles in aggregates (N_p) generated in the paddle mixer to aggregate areas.

Fractal dimensions can also be calculated from the size distributions of coagulating systems using two different methods: steady-state size distributions and a two slope method requiring two different instruments to measure size distributions. The steady-state method is based on a dimensional analysis that assumes there is a continuous source of primary particles through the size distribution used to form the aggregates, and a continuous loss of particles through sedimentation (Friedlander 1960a, b, 1977). Hunt showed that slopes of particle size distributions observed in the ocean (Hunt, 1980) and in laminar shear devices during coagulation of clay particles (Hunt, 1982) were consistent with theoretical predictions derived from a dimensional analysis. Jiang and Logan (1991) extended this analysis using fractal geometrical properties of aggregates and showed that fractal dimensions could be calculated from the slopes of log–log plots. For example, for shear coagulation, they derived the steady-state relationships:

$$s_v = -\frac{3}{2}\left(1 + \frac{1}{D_3}\right) \tag{6}$$

$$s_l = -\frac{1}{2}\left(1 + \frac{3}{D_3}\right), \tag{7}$$

where s_v is the slope of a discrete particle size distribution, $n(v)$, as a function of solid volume, v, and s_l is the slope of the discrete particle size distribution, $n(l)$, as a function of maximum aggregate length. These equations can be rearranged and solved for D_3 as a function of the size distribution slopes. A similar set of relationships were derived by Jiang (1993) based on the cumulative size and volume distribution, $N(l)$ and $N(v)$, based on the slopes in log–log plots of particle size or volume, S_l or S_v, for shear and differential sedimentation mechanisms (Table 2). Unless stated otherwise, all calculations for fractal dimensions generated by differential sedimentation were based on the assumption that $D_2 = D_3$ and $b = 1.0$. As a result, the equations given for differential sedimentation reduce to the same equation for coagulation by fluid shear (Table 2).

Calculation of a fractal dimension does not require an assumption of steady state conditions if both the size and volume distributions are known for the same population of particles and if the fractal dimension is unchanged over the size distribution considered. The size and volume distributions can be represented by two power law relationships (Jiang and Logan, 1991):

$$n(l) = A_l l^{s_l} \tag{8}$$

$$n(v) = A_v v^{s_v}, \tag{9}$$

Table 1. Properties of aggregates from fractal geometry*

Property	Equation	Scaling relationship
Solid volume, v	$v = \psi^{D_3/3}\xi_0 l_0^{3-D_3} l^{D_3}$	$V \propto l^{D_3}$
Encased volume, v_c	$v_c = \xi l^3$	$v_c \propto l^3$
Mass, m	$m = \rho_0 \psi^{D_3/3}\xi_0 l_0^{3-D_3} l^{D_3}$	$m \propto l^{D_3}$
Density, ρ	$\rho = \rho_0 \psi^{D_3/3}\frac{\xi_0}{\xi}\left(\frac{l}{l_0}\right)^{D_3-3}$	$\rho \propto l^{D_3-3}$
Porosity, ϵ	$\epsilon = 1 - \psi^{D_3/3}\frac{\xi_0}{\xi}\left(\frac{l}{l_0}\right)^{D_3-3}$	$\epsilon \propto l^{D_3-3}$
Settling velocity, U	$U = \left[\frac{2g\xi_0(\rho_0-\rho_w)\psi^{D_3/3} l_0^{1+D_2-D_3} \nu^{-b}}{a\rho_w\xi_2} l^{D_3+b-D_2}\right]^{1/(2-b)}$	$U \propto l^{(D_3+b-D_2)/(2-b)}$

*ζ_0 and ξ_0 are the packing and shape factors of primary particles in the aggregate of size l_0 and density ρ_0, ζ and ξ the packing and shape factors of the aggregate, g the gravitational constant, ρ_w the density of water, $\psi = \zeta\xi/\xi_0$, and a and b are constants relating the drag coefficient of spheres to the Reynolds number. For $Re \leq 0.1$, $a = 24$ and $b = 1$, and for $0.1 < Re < 10$, $a = 29.0$, and $b = 0.871$ [See Jiang and Logan (1991) for details].

Table 2. Three-dimensional fractal dimension as a function of the type of size distribution and the coagulation mechanism

Basis	Distribution type	Fractal dimension, D_3		
		Shear	Differential sedimentation	Mechanism independent
Steady state				
	Discrete volume	$\frac{-3}{2s_v+3}$	$\frac{D_2+b-4}{s_v(4-2b)-3b+7}$	
	Cumulative, volume	$\frac{-3}{2S_v+1}$	$\frac{D_2+b-4}{S_v(4-2b)-b+3}$	
	Discrete, length	$-(2s_l+5)$	$\frac{s_l(2b-4)+3b+D_2-8}{3-b}$	
	Cumulative, length	$-(2S_l+3)$	$\frac{S_l(2b-4)+b+D_2-4}{3-b}$	
Non-steady state				
	Discrete, both volume and length			$\frac{1+s_l}{1+s_v}$
	Cumulative, both volume and length			$\frac{S_l}{S_v}$

where A_l and A_v are the proportionality constants. From fractal geometry calculations relating aggregate size and length (Table 1),

$$v = \psi^{D_3/3}\ \xi_0\ l_0^{3-D_3}\ l^{D_3} \tag{10}$$

where ψ is a constant aggregate shape and packing factors, l_0 is the size of primary particles and ξ_0 is a shape factor of primary particles in the aggregate (Jiang and Logan, 1991). If we analyze the same population of particles for both size and volume, and use the relationship of $n(l) = n(v)\,dv/dl$, from equations (8)–(10) we have the equality:

$$A_l l^{s_l} = \psi^{D_3/3}\xi_0\ l_0^{3-D_3}\ l^{D_3-1}\ D_3\ A_v\ v^{s_v} \tag{11}$$

Using only the proportionality from equation 11,

$$l^{s_l} \sim l^{D_3-1}\ l^{D_3 s_v}. \tag{12}$$

Therefore, D_3 can be determined from equation (12) as:

$$D_3 = \frac{s_l+1}{s_v+1}. \tag{13}$$

Since these equations do not require the assumption of a steady state or stationary size distribution, the fractal dimension can be calculated without having to assume a steady state size distribution if $n(v)$ and $n(l)$ can be measured simultaneously using different types of instruments. A similar equation can be derived based on the slopes obtained from cumulative size distributions (Table 2).

EXPERIMENTAL

Particles

Fluorescent carboxylate microspheres (type YG, Polysciences Inc.) were used because of their constant size ($0.92 \pm 0.01\ \mu$m), low density (1.055 g cm^{-3}), initial monodispersivity, chemical resistance, and ability to be destabilized by salts. Microspheres were stored in a solution of deionized water at a concentration of approximately 5.81×10^{10} ml^{-1}, and diluted into artificial seawater (Riley and Skirrow, 1965) to an initial concentration of 4×10^6 ml^{-1} for coagulation experiments.

Particle stability was minimized by varying NaCl concentrations to obtain the minimum collision efficiency, α, defined here as a ratio of the measured collision rate divided by the collision rate calculated using a rectilinear coagulation model. For shear coagulation, α can be calculated from

$$\alpha = \frac{1}{k_{th}t}\ln\left(\frac{N_p}{N_{po}}\right), \tag{14}$$

where N_{po} and N_p(ml^{-1}) are the initial and final number concentration of particles, k_{th} the predicted collision reaction constant, and t time. For turbulent shear, k_{th} is calculated using $2.2\,\Phi G$, where Φ is the solid volume fraction of particles and G the shear rate. This equation is only valid for the initial coagulation period of a monodisperse system and it has been experimentally verified by Birkner and Morgan (1964). Collision efficiencies in the paddle mixers increased from $\alpha = 0.0023$ (0.05 M) to the maximum collision efficiency of $\alpha = 0.24$ in the artificial seawater solution. All experiments were conducted with fully destabilized particles, and further chemical characterization of the beads was not warranted.

Mixing devices

Microspheres were coagulated at room temperature (23°C) using either a paddle mixer or a roller cylinder apparatus. The paddle mixer (Phipps and Bird Six Paddle Stirrer, model 7790-400) consisted of six stainless steel stirring paddles (3–8 cm long, 19.2 cm^2 surface area) mounted in a frame and driven by a variable speed electric motor set at a paddle rotation speed of 30 rpm. Microsphere solutions were placed in 1 l glass beakers filled to 800 ml. Paddle heights were adjusted to mid-depth of the solution. Based on a comparison of coagulation rates of monodisperse spheres in a couette (laminar shear) device with coagulation rates observed in the paddle mixer under identical conditions, it was estimated that the shear rate in the paddle mixer was 10 s^{-1} (Jiang and Logan, 1994).

The rolling cylinder apparatus consisted of two rollers mounted horizontally on a frame as described by Shanks and Edmondson (1989). A variable speed electric motor drove one roller, and the other roller spun freely. The

position of the free spinning roller was adjustable to accommodate different cylinder sizes, although all experiments were conducted using 60 ml glass bottles (4 cm diameter) with straight ends, wide mouths, and teflon lined (Dyn-A-Med) screw caps. Small diameter bottles were used to minimize fluid shear to $< 1\ s^{-1}$ during initial start up (~ 10 min) in the bottles. These shear rates and initial mixing times are based on calculations by for 3.25 cm diameter bottles by Jackson (1994). Bottles were completely filled by capping them while submerged in a 1 l beaker filled with the microsphere-seawater solution. This procedure avoided entrapment of any air bubbles which would interfere with solid body rotation of the solution within the bottles. The filled bottles were then placed on the apparatus and rotated at 7.5 rpm.

Samples

Microsphere aggregates from each device were sampled by pipet (0.1–1 ml) and filtered onto 0.2 μm polycarbonate membrane filters (0.2 μm, prestained black, Poretics Corp.), placed on clear slides and covered with immersion oil and a cover slip. The slides were then analyzed for particle size distributions using the image analysis system. A separate sample was taken for analysis of volume distributions using a particle counter.

Size distributions by aggregate length

Slides containing fluorescent microsphere aggregates were analyzed using an image analysis system connected to a microscope (Olympus BH-2) equipped with a mercury lamp (Chiu Technical Corporation Mercury-100) and filters for blue light. The image analysis system used consisted of a video camera, monitor (512 × 512 pixels), and a personal computer containing image analysis software (Olympus Cue-2). Aggregate size distributions were calculated using maximum aggregate lengths. Viewing fields were selected at random on the slides (at 400×) until a minimum of 800 analyzed aggregates accumulated for each sample. Aggregates with maximum diameters less than 3.0 μm were excluded from analyses to match the size range analyzed by the particle counter. Aggregate properties used for analysis were maximum size, projected area and perimeter.

Analyses of aggregates for boundary fractal dimensions (Kaye, 1991) were performed separately by analyzing individual randomly selected aggregates at 1000× power using the image analysis system and a computer program developed by Jiang (1993). This program generated several different box sizes that encased the aggregate perimeter, and provided the one-dimensional boundary fractal dimension based on equation (3).

Size distributions by aggregate volume

Unfiltered portions of microsphere aggregate samples were analyzed with an Elzone 180 resistance-type particle counter (Particle Data, Inc.) equipped with a 48 μm orifice tube and a 200 μl volumetric tube. The conductive fluid used in the particle counter and for sample dilution was a 3% NaCl-distilled water solution filtered twice through 0.2 μm polycarbonate membrane filters. Calibrations were performed with standardized 5 μm and 15 μm latex microspheres. Set at log 10 scale, the lower measurable aggregate size was 3 μm. Samples were diluted to a level where a minimum of 2000 aggregates were analyzed without excess coincidence.

Size distribution formats

Aggregate properties have been determined either using all data (Alldredge and Gotschalk, 1988) or by condensing data into different size classes (Logan and Wilkinson, 1990). Since fractal dimensions calculated from size distributions can be very sensitive to errors in the slopes of the distribution, we calculated slopes of size distributions using three methods: discrete size distributions using all data, discrete size distributions using data averaged into different particle sizes, and cumulative size distributions using all data.

RESULTS

Power-law fractal dimensions

Aggregated samples from the paddle mixer were collected for analysis after 36 h of coagulation. Larger aggregates that had settled onto the container bottom and the smallest aggregates ($< 3\ \mu$m) were excluded from the analysis. A total of 823 aggregates ranging from 3 to 70 μm were used to calculate fractal dimensions of $D_1 = 1.19 \pm 0.01$ and $D_2 = 1.89 \pm 0.02$ (Table 3) from log–log plots of length and perimeter or area (Fig. 1). A boundary fractal dimension of $D_{1b} = 1.49 \pm 0.02$ was calculated using 25 randomly selected aggregates.

Coagulation rates were much lower in the rolling cylinders than in the paddle mixer. Although the water in the paddle mixers became clear after 3 d, the water in the rolling cylinders remained cloudy even after 8 d when samples were collected. When the contents of the roller was examined before sampling, there appeared to be a much less continuous size distribution of aggregates. A few very large aggregates (~ 20 mm) were observed in the roller, but we did not attempt to sample these largest aggregates. Samples obtained from the roller contained aggregates ranging in size from only 3 to 13 μm. Fractal dimensions of $D_1 = 1.14 \pm 0.01$ and $D_2 = 1.68 \pm 0.02$ (Table 3) were calculated from log–log plots of length and perimeter or area (Fig. 1c,d) based on analysis of 2,102 aggregates, and a fractal dimension of $D_{1b} = 1.42 \pm 0.06$ was calculated for a subset of 25 aggregates.

The lower D_2 fractal dimensions of the rolling cylinder indicates that aggregates of these aggregates were more amorphous and less compact than those produced in the paddle mixer. However, both of the one dimensional fractal dimensions for the rolling cylinder were also lower than the equivalent paddle mixer values. Since the one dimensional fractal dimension increases with the irregularity of a boundary, the fractal nature of the aggregate perimeters was not correlated with changes in aggregate area. A similar lack of correlation between trends in D_2 and

Table 3. Power law fractal dimensions of aggregates produced in paddle mixer and rolling cylinder devices

Equation number	Fractal dimension	Paddle mixer	Rolling cylinder
4	D_1	1.19 ± 0.01 ($n = 823$; $r^2 = 0.96$)	1.14 ± 0.01 ($n = 2, 102$; $r^2 = 0.89$)
3	D_{1b}	1.49 ± 0.02 ($n = 25$)	1.42 ± 0.06 ($n = 25$)
1	D_2	1.89 ± 0.02 ($n = 823$; $r^2 = 0.98$)	1.68 ± 0.02 ($n = 2, 102$; $r^2 = 0.75$)

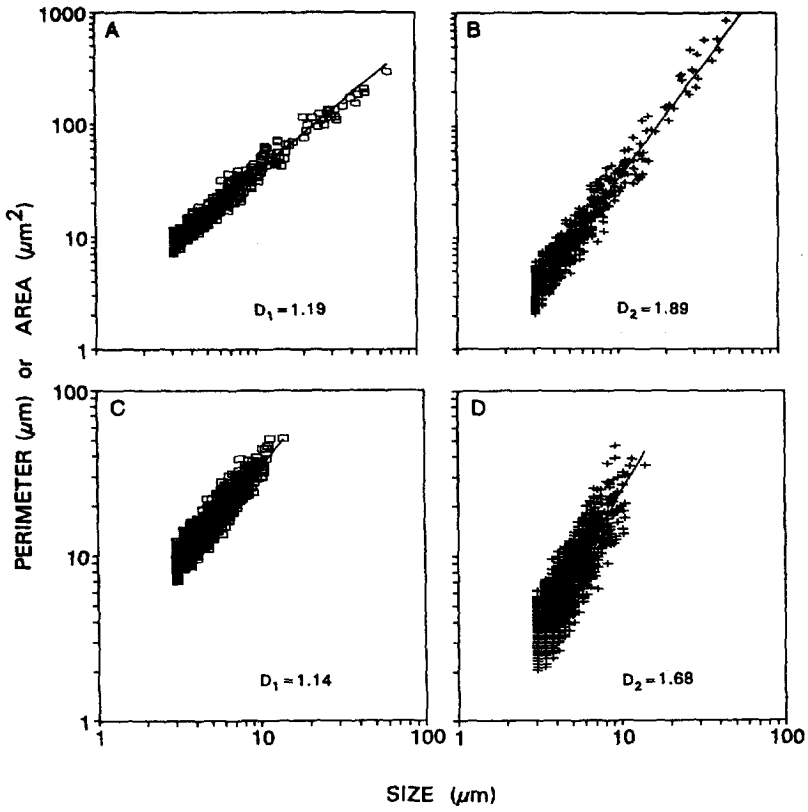

Fig. 1. Aggregate perimeter (□) and area (+) as a function of aggregate size (maximum length) measured using an image analysis system for aggregates generated in a paddle mixer (A and B) and in a rolling cylinder (C and D). The slopes of the regression lines are equal to the fractal dimensions D_1 and D_2 based on perimeter and area, respectively.

D_1 fractal dimensions has been previously found for marine snow aggregates (Kilps *et al.*, 1994).

A subset of smaller aggregates obtained from paddle mixer was used to test the hypothesis that the two and three dimensional fractal dimensions were equal. The number of primary particles in 200 aggregates and the area from the image analysis system were compared using equation (5) (Fig. 2). The slope of the line from the log–log plot was $(D_2/D_3) = 0.99 \pm 0.01$, indicating that the two dimensional fractal dimensions shown in Table 3 were also equal to D_3.

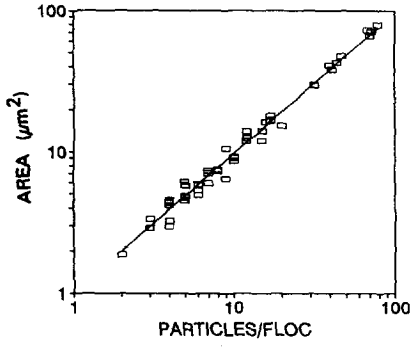

Fig. 2. Cross-sectional area of aggregates produced in the paddle mixer measured using the image analysis system as a function of the number of particles in the aggregate. The slope of the regression line is 0.99 ± 0.01 indicating that the two- and three-dimensional fractal dimensions are equal.

Fractal dimensions from size distributions

Paddle mixer. Size distributions were analyzed using three different distribution formats in order to determine the differences in the magnitude and error of the calculated three dimensional fractal dimensions. All three methods indicated data from the image analysis system on maximum size and number concentration were linear and least scattered in the range of 3–10 μm (Fig. 3). Above 10 μm, the discrete size distribution data were very scattered (Fig. 3a). When data were averaged into size classes (Fig. 3b) there was an insufficient number of aggregates larger than 40 μm to determine if the slope of the line was changing for aggregates larger than 20 μm, or if there was actually a slope change. Size distribution data plotted as a continuous distribution (Fig. 3c) did not resolve this question.

Volume-size distributions obtained with the particle counter also produced a similar trend in data with distribution format (Table 4). The cumulative size distribution format resulted in the least variation

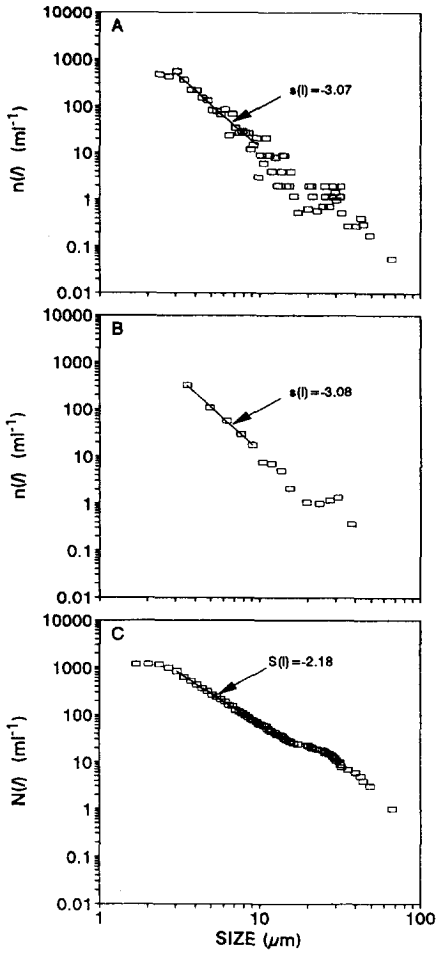

Fig. 3. Maximum length size distributions of aggregates (□) produced in the paddle mixer analyzed using the image analysis system prepared using different size distribution formats: (A) discrete, (B) discrete averaged, and (C) cumulative. Lines produced by linear regression indicate the range of particle sizes used to calculate the indicated slopes.

in slope compared to the discrete and discrete-averaged methods.

It was difficult to directly compare the size distributions from the two instruments since the image analysis system produces aggregate length and the particle counter aggregate volume. However, for the smallest aggregates we could relate aggregate volume, from counting the number of primary particles in an aggregate, and aggregate size. To interrelate size and volume we defined the smallest particle of length of 3.0 μm to have a total volume of 4.46 μm^3. Using this point, we were able to draw a size-volume slope using either the Euclidean value of 3 or a fractal dimension 1.89 based on the power law relationships for these aggregates. This produced estimates of aggregate size from volume measurements in the particle counter that could be compared to particle sizes obtained using the image analysis system.

Based on particle sizes obtained from the volume-size equation and $D_3 = 1.89$, the change in slope in Fig. 4a occurs at about an aggregate size of 50–60 μm. Because the particle counter orifice used in these experiments was only 48 μm, we concluded that the larger volume-size distribution data were probably unreliable due to distortion of aggregates pulled through the small orifice. Therefore, we did not use any particle distribution data for aggregates in the larger size ranges. The linearity of the slopes shown in Fig. 4 for the volume–size distributions provide evidence that we were comparing similar size distributions from the image analysis and particle counter techniques and that we were analyzing particles in a similar size range.

The slopes from the size distributions for the smaller aggregates were used to calculate fractal dimensions based on the appropriate equations using either aggregate length or volume. Within the standard error of the slope, the fractal dimensions for each technique were equal, but the cumulative size distribution produced the least error in D_3. For example, based on the equations for steady-state coagulation, three-dimensional fractal dimensions were 1.15 ± 0.77 and 1.15 ± 0.26 using the slopes from the discrete and discrete-averaged size distributions for aggregate size (Table 4). However, the error for $D_3 = 1.35$ was only ± 0.06 based on the cumulative distribution. Since the same data was used in this analysis, the reduction of error results from smoothing out of data by using a cumulative size distribution and not an improved experimental technique.

Steady-state fractal dimensions of $D_3(l) = 1.35 \pm 0.06$ and $D_3(v) = 2.38 \pm 0.08$ were calculated using cumulative size distributions. The lack of agreement between the steady-state three-dimensional fractal dimensions for all three size distribution formats indicates that the system was not at steady-state.

Table 4. Three-dimensional fractal dimensions of microsphere aggregates calculated from size distributions: paddle mixer

	Fractal dimensions from size distributions		
	Coagulation by shear or differential sedimentation, (assuming steady-state)		Mechanism independent (non-steady-state)
	$D_3(l)$	$D_3(v)$	$D_3(l, v)$
Discrete	1.15 ± 0.77	2.45 ± 0.06	1.86 ± 0.53
Discrete-averaged	1.16 ± 0.26	2.51 ± 0.06	1.89 ± 0.29
Cumulative	1.35 ± 0.06	2.37 ± 0.04	1.92 ± 0.04

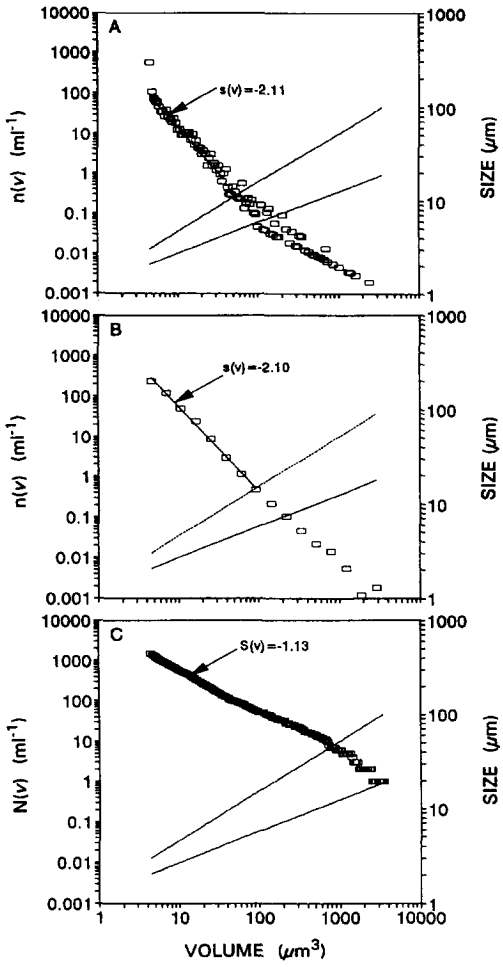

Fig. 4. Volume size distributions of aggregates (□) produced in the paddle mixer analyzed using the particle counter prepared using different size distribution formats: (A) discrete, (B) discrete averaged, and (C) cumulative. Solid lines indicate the range of particle sizes used to calculate the indicated slopes. To convert particle volume to size read the aggregate size from the right axis based on particle volume using either the line based on $D_3 = 3.0$ (...) or $D_3 = 1.89$ (– –).

Analysis of the cumulative size distributions from both instruments using the two slope method produced a fractal dimension of $D_2(l, v) = 1.92 \pm 0.04$ for aggregates produced in the paddle mixer. Fractal dimensions having similar values, but larger errors, were calculated using the discrete and discrete-averaged size distributions. Since the two-slope technique is independent of coagulation mechanisms, we concluded from this analysis that $D_3(l, v) = 1.92 \pm 0.04$ for aggregates produced in the paddle mixer.

Rolling cylinder. Steady state fractal dimensions calculated using the discrete, discrete-averaged and cumulative size distributions (Table 5) all showed similar patterns with technique as observed above for the paddle mixer aggregates. Discrete and discrete-average values of D_3 were similar in magnitude, but had higher errors, than those calculated using cumulative size distributions. Fractal dimensions based on steady-state equations for aggregate size did not agree with values based on volume, indicating that size distributions produced in the roller could not be considered to be at steady-state. Based on the non-steady-state analysis, we concluded that aggregates produced in the roller had a three-dimensional fractal dimension of $D_3 = 1.59 \pm 0.16$.

Unlike the cumulative size distribution observed for aggregates produced in the paddle mixer, the maximum length size distribution produced in the roller bottle was curved over the whole region and displayed no linear portion (Fig. 5a). The volume size distribution was linear over the smaller size range, but changed slope abruptly at a volume of 200–400 μm^3. Based on the two slope fractal dimension of $D_3 = 1.59$ for these aggregates, this change in slope corresponds to an aggregate size of $\sim 10\ \mu m$. The second nearly linear portion covers a size range of 10–100 μm, a range which is inconsistent with measurements made using only a 48 μm orifice diameter on the particle counter. Therefore, we used only the smaller size ranges to calculate fractal dimensions (Table 5).

DISCUSSION

Two- and three-dimensional fractal dimensions calculated from the power law equations and size distributions indicate that aggregates produced in the rolling cylinder are more fractal than aggregates generated in the paddle mixer. Using aggregate size and area, aggregates from the paddle mixer had $D_2 = 1.89 \pm 0.02$, while aggregates in the rolling cylinder had $D_2 = 1.68 \pm 0.02$. From fractal geometry, if $D_3 \leq 2$, then $D_3 = D_2$ (Meakin, 1988). Agreement between the two different methods makes it unlikely that the fractal dimension of the particles changed over the size ranges investigated in this study. Since the three dimensional fractal dimensions calculated in this study were less than two, and since the image

Table 5. Three-dimensional fractal dimensions of microsphere aggregates calculated from size distributions: rolling cylinder

	Fractal dimensions from size distributions		
	Coagulation by shear or differential sedimentation, (assuming steady-state)		Mechanism independent (non-steady-state)
	$D_3(l)$	$D_3(v)$	$D_3(l, v)$
Discrete	2.51 ± 1.13	0.83 ± 0.05	1.19 ± 0.30
Discrete-averaged	2.44 ± 1.79	0.75 ± 0.08	1.08 ± 0.45
Cumulative	2.31 ± 0.65	0.83 ± 0.07	1.59 ± 0.16

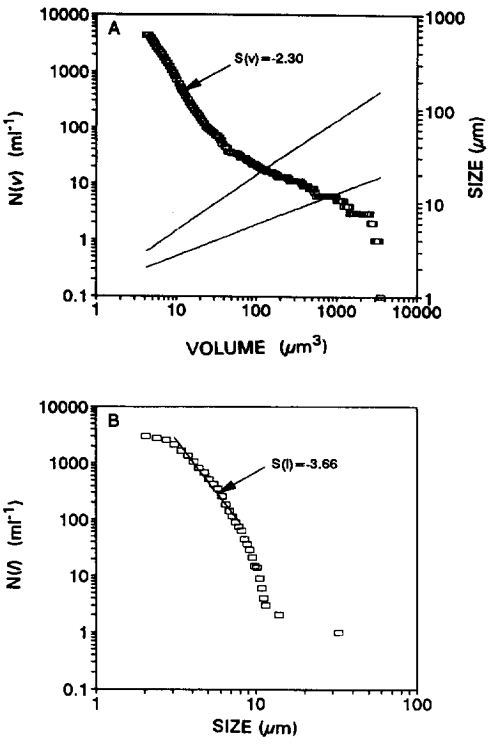

Fig. 5. Cumulative size distributions of aggregates (□) produced in the rolling cylinder device using the (A) image analysis system, and (B) particle counter (— regression line; ... size based on $D_3 = 3.00$; ––– size based on $D_3 = 1.59$). See Fig. 4 caption for explanation of lines.

analysis results supported that $D_2 = D_3$, then D_2 obtained from the power law scaling method should be equal to D_3 using the size distribution methods if both methods accurately quantify aggregate properties. The fractal dimensions produced using the two-slope method and the cumulative size distributions were $D_3(l, v) = 1.92 \pm 0.04$ and $D_3(l, v) = 1.59 \pm 0.16$, for the paddle mixer and rolling cylinder, respectively. Within the errors of the fractal dimensions, these two different methods produced similar fractal dimensions.

Fractal dimensions calculated by assuming a steady-state condition existing within the coagulation devices were not in agreement with values calculated using the non-steady-state method, indicating that steady state conditions did not exist within the devices at the time samples were obtained. For example, fractal dimensions using cumulative size distributions and assuming steady state were in the paddle mixer were $D_3(l) = 1.35 \pm 0.06$ and $D_3(v) = 2.37 \pm 0.04$ based on size and volume. If the system had been at steady-state, then these values would have both been equal to the non-steady-state result of $D_3(l, v) = 1.92 \pm 0.04$. Other experiments in our laboratory using a concentric cylinder device to produce coagulation under laminar shear conditions suggests that long times (on the order of days to weeks) are necessary before steady state and non-steady state fractal dimensions calculated from size distributions become equal (Jiang, 1993).

The magnitude of D_3 calculated from size distributions was not affected by the distribution format. However, the errors associated with the slopes decreased in the order discrete, discrete-averaged and cumulative. Fractal dimensions calculated from size distributions are very sensitive to errors in slopes (Jiang and Logan, 1991). Thus, the best method of calculating fractal dimensions is probably to use cumulative size distributions since this technique produces the most reliable slopes for the calculation.

We cannot resolve whether the aggregates produced in the coagulation devices were generated by shear motion or differential sedimentation because the equations used to calculate these fractal dimensions are identical for both coagulation mechanisms when $D_2 = D_3$ and $b = 1$ (Table 2). Moreover, a recent study by Jackson (1994) challenges whether aggregates produced in rolling cylinders are generated by encounters in the fluid or are strongly influenced by collisions with the container walls. Jackson analyzed particle motion in a rolling cylinder during the initial period of time after a roller was started and found that particles suspended in the fluid could settle and strike the container walls. As a result, it is likely that some aggregates were generated in the rolling cylinder by fluid shear and by particles hitting each other on the container walls. It is clear that coagulation mechanisms in the rolling cylinder need to be further investigated.

The characteristics of the size distributions produced in the two different coagulation devices may help explain differences in the resulting fractal dimensions, particularly with regard to wall effects in the rolling cylinders. It has to be recognized that all coagulation devices suffer from some limitations and fail to generate aggregates under well controlled fluid mechanical conditions. The paddle mixer, for example, produces much higher shear rates near the paddle tips than near the walls (Tomi and Bagster, 1978). Aggregate restructuring can occur over time due to particles in the aggregate sticking to each other. Such a process increases the fractal dimension of colloidal aggregates. High shear rates in the paddle mixer device, particularly in the vicinity of the paddle tip, may have caused aggregate restructuring and increased in the fractal dimensions of aggregates. Although $D_3(l, v) = 1.92$ was larger than the fractal dimension observed for diffusion limited aggregation of colloidal particles ($D_3 = 1.8$), this value is still lower than fractal dimensions of $D_3 = 2.2$ measured for colloids formed by Brownian motion under reaction-limited conditions.

Aggregate size distributions measured in the rolling cylinder were unusual for several reasons. Although very large (~ 20 mm) aggregates were observed in the rolling cylinder, we found very few aggregates larger than $\sim 15\ \mu$m resulting in a discontinuous size distribution for larger particles in the roller bottle. We

believe that the loss of intermediate sized aggregates was due to rapid coagulation in the rolling cylinder of aggregates near the upward side of the container. When we observed particle motion through the clear roller bottle sides, we noticed that large aggregates in the roller bottle would strike the bottom of the container and, during the upward rotation, would move only slightly away from the side of the container before settling back down onto the container surface. This motion of large aggregates scavenged other particles from the container and removed aggregates before they could grow to very large sizes.

Size distributions produced in the roller bottles were also curved, and not straight lines, on cumulative size distribution plots based on aggregate length (Fig. 5). This curvature indicates that aggregate concentrations in larger size classes ($>10\,\mu$m) were reduced below values based on the abundance of smaller aggregates. This reduction in aggregate concentration also suggests that particles that would normally have been present in a continuous size distribution were absent from the roller. Thus, we conclude that the size distribution was altered, and discontinuous, because of the scavenging role of larger aggregates.

The range in fractal dimensions of 1.59 to 1.92 is typical of fractal dimensions calculated in other studies for aggregates formed in the ocean, although aggregates made from a variety of different types of particles can have lower values (Table 6). The earliest estimates of fractal dimensions, based on size-porosity data, indicated fractal dimensions of $D_3 = 1.52 \pm 0.19$ for diatom aggregates, and 1.39 ± 0.15 for general marine snow aggregates (Logan and Wilkinson, 1990). Kilps *et al.* (1994) analyzed photographs of marine snow particles and found a fractal dimension of $D_2 = 1.72 \pm 0.07$ when aggregates of diatoms, amorphous particles, fecal pellets, and miscellaneous debris were analyzed as a combined group (Table 6). Analyzed separately, the diatom snow aggregates had the highest fractal dimension of $D_2 = 1.86 \pm 0.13$, and miscellaneous debris the lowest fractal dimension of 1.28 ± 0.11.

The first set of fractal dimensions derived from size distributions were based on the assumption that $b = 1$ (Jiang and Logan, 1991) since marine snow sized particles were not included in the analysis. The volume-size distribution slopes of particles larger than $40\,\mu$m in the ocean gathered from other studies ranged from -2.22 to -2.43 (Jiang and Logan, 1991). Assuming that $D_2 = D_3$ and $b = 1$, Jiang and Logan calculated a range of $D_3 = 1.61$ to 2.08. However, if we assume a continuous size distribution for larger particles, these slopes of particle size distributions for oceanic particles can be extended and used to calculated fractal dimensions for marine snow sized particles. Marine snow sized aggregates can have Reynolds numbers larger than 0.1 (Alldredge and Gotschalk, 1988), and therefore for these particles we can use a value of $b = 0.871$ (Jiang and Logan, 1991). This results in fractal dimensions in the range of $D_3(v) = 1.48$ to 1.93, a range which provide better agreement with fractal dimensions obtained for marine snow sized particles in other studies using different techniques (Table 6).

The comparison of these different studies makes it evident that marine snow particles can have a range in fractal dimensions based on the type of particles forming the aggregate. Unfortunately, it still is not apparent whether this range results from the different types of particles making the aggregate or from different mechanisms of coagulation. The current study provides evidence that the fluid mechanical conditions can alter the aggregate geometry, since aggregates formed in the rolling cylinder had lower fractal dimensions than aggregates from the paddle mixer. Therefore, although neither of these devices precisely reproduces the conditions in the ocean, it has been shown through the use of identical particles in different devices that the fluid mechanical environment can alter the structure of the aggregates, and produce D_3 values less than those observed for colloidal aggregates.

The size distribution data presented here provide additional evidence that size distributions require manipulation using fractal scaling properties if they are converted from mass, area or volume to size. Size

Table 6. Comparison of fractal dimensions determined using different techniques

Aggregate type	Method	Fractal dimension	Reference
Marine snow			
Diatoms	Power law (size-porosity)	$D_3 = 1.39 \pm 0.15$	a
General	Power law (size-porosity)	$D_3 = 1.52 \pm 0.19$	a
Diatoms	Power law (size-area)	$D_2 = 1.86 \pm 0.13$	b
Amorphous	Power law (size-area)	$D_2 = 1.63 \pm 0.72$	b
Fecal pellets	Power law (size-area)	$D_2 = 1.34 \pm 0.16$	b
Miscellaneous	Power law (size-area)	$D_2 = 1.28 \pm 0.11$	b
Ocean particles			
$>40\,\mu$m	Size distribution ($b = 1.0$)	$D_3(v) = 1.61$–2.08	c
$>40\,\mu$m	Size distribution ($b = 0.87$)	$D_3(v) = 1.48$–1.93	c
Microspheres			
Paddle mixer	Size distributions ($b = 1.0$)	$D_3(l, v) = 1.92 \pm 0.04$	d
Paddle mixer	Power law (size-area)	$D_3 = 1.89 \pm 0.02$	d
Rolling cylinder	Size distributions ($b = 1.0$)	$D_3(l, v) = 1.59 \pm 0.16$	d
Rolling cylinder	Power law (size-area)	$D_3 = 1.68 \pm 0.02$	d

a, Logan and Wilkinson, 1990; b, Kilps *et al.*, 1994; c, Jiang and Logan, 1991; d, this study.

distribution data obtained from the literature on aggregates sizes obtained from photographic, laser or resistance particle counters should, therefore, be carefully examined for the basis of the size calculations before the results are used.

Acknowledgements—We thank G. A. Jackson and Q. Jiang for comments on the manuscript. Funding was provided by ONR Grant N00014-91-J-1249.

REFERENCES

Alldredge A. L. and Gotschalk C. (1988) *In situ* settling behavior of marine snow. *Limnol. Oceanogr.* **33,** 339–351.

Alldredge A. L. and Silver M. W. (1988) Characteristics, dynamics and significance of marine snow. *Prog. Oceanogr.* **20,** 41–82.

Alldredge A. L., Passow U. and Logan B. E. (1993) The central role of transparent mucopolysaccharide particles in marine aggregation. *Deep-Sea Res.* **40,** 1131–1140.

Birkner F. B. and Morgan J. J. (1964) Polymer flocculation kinetics of dilute colloidal suspensions. *J. AWWA* **60,** 175–191.

Burrough P. A. (1989) Fractals and geochemistry. In *The Fractal Approach to Heterogeneous Chemistry* (Edited by Avnir D.), pp. 383–406. John Wiley, New York.

Fowler S. W. and Knauer G. A. (1986) Role of large particles in transport of elements and organic compounds through the oceanic water column. *Prog. Oceanogr.* **16,** 60–68.

Friedlander S. K. (1960a) On the particle-size spectrum of atmospheric aerosols. *J. Meteorol.* **17,** 373–374.

Friedlander S. K. (1960b) Similarity considerations for the particle-size spectrum of a coagulating, sedimenting aerosol. *J. Meteorol.* **17,** 479–483.

Friedlander S. K. (1977) *Smoke, Dust and Haze: Fundamentals of Aerosol Behavior.* Wiley-Interscience: New York.

Hill P. S. (1992) Reconciling aggregation theory with observed vertical fluxes following phytoplankton blooms. *J. Geophys. Res.* **97,** 2295–2308.

Hunt J. R. (1980) Prediction of oceanic particle size distributions from coagulation and sedimentation mechanisms. In *Advances in Chemistry Series No. 189. Particulates in Water* (Edited by Kavanaugh M. C. and Leckie J. O.), pp. 243–257. American Chemical Society, Washington DC.

Hunt J. R. (1982) Self-similar particle size distributions during coagulation: theory and experimental verification. *J. Fluid Mech.* **122,** 303–309.

Jackson G. A. (1990) A model of the formation of marine algal flocs by physical coagulation processes. *Deep-Sea Res.* **37,** 1197–1211.

Jackson G. A. (1994) Particle trajectories in a rotating cylinder: implications for aggregation incubations. *Deep-Sea Res.* **41,** 429–437.

Jiang Q. (1993) Fractal structure of aggregates induced by shear motion. Ph.D. dissertation, University of Arizona, Tucson.

Jiang Q. and Logan B. E. (1991) Fractal dimensions of aggregates determined from steady-state size distributions. *Environ. Sci. Technol.* **25,** 2031–2038.

Jiang Q. and Logan B. E. (1994) Fractal dimensions of aggregates produced in laminar and turbulent shear devices (submitted).

Kaye B. H. (1989) Image analysis techniques for characterizing fractal structures. In *A Fractal Approach to Heterogeneous Chemistry* (Edited by Avnir D.), pp. 55–66. John Wiley, New York.

Kilps J. R., Logan B. E. and Alldredge A. L. (1994) Fractal dimensions of marine snow aggregates determined from image analysis of *in situ* photographs *Deep-Sea Res.* **41,** 1159–1169.

Kiørboe T., Anderson K. P. and Dam H. G. (1990) Coagulation efficiency and aggregate formation in marine phytoplankton. *Mar. Biol.* **107,** 235–245.

Li D.-H. and Ganczarczyk J. J. (1989) Fractal geometry of particle aggregates generated in water and wastewater treatment processes. *Environ. Sci. Technol.* **23,** 1385–1389.

Lin M. Y., Lindsay H. M., Weitz D. A., Ball R. C., Klein R. and Meakin P. (1989) Universality in colloid aggregation. *Nature* **339,** 360.

Logan B. E. and Wilkinson D. B. (1990) Fractal geometry of marine snow and other biological aggregates. *Limnol. Oceanogr.* **35,** 130–136.

Logan B. E. and Wilkinson D. B. (1991) Fractal dimensions and porosities of *Zoogoloea ramigera* and *Saccharomyces cerevisae* aggregates. *Biotechnol. Bioengng.* **38,** 389–396.

McCave I. N. (1975) Vertical flux of particles in the ocean. *Deep-Sea Res.* **22,** 491–502.

Meakin P. (1988) Fractal aggregates. *Adv. Colloid Inter. Sci.* **28,** 249–331.

Pasciak W. J. and Gavis J. (1975) Transport limited nutrient uptake rates in *Ditylum brightwelli. Limnol. Oceanogr.* **20,** 604–616.

Riley J. P. and Skirrow G. (1965) *Chemical Oceanography,* Vol. 1. Academic Press, London.

Shanks A. L. and Edmondson E. W. (1989) Laboratory-made artificial marine snow: a biological model of the real thing. *Mar. Biol.* **101,** 463–470.

Tomy D. T. and Bagster D. F. (1978) The behaviour of aggregates in stirred vessels. Part I—theoretical considerations on the effects of agitation. *Trans. I. Chem. E.* **56,** 1–8.

Tooby P. F., Wick G. L. and Isaacs J. D. (1977) The motion of a small sphere in a rotating velocity field: a possible mechanism for suspending particles in turbulence. *J. geophys. Res.* **82,** 2096–2100.